Manuscript Draft

Title: Octahedral and Trigonal-Prismatic Coordination Preferences in Nb-, Mo-, Ta-, and W-based ABX_2 Layered Oxides, Oxynitrides, and Nitrides

Type of Manuscript: Article

Authors: Akira Miura[a]*, Kiyoharu Tadanaga[a], Eisuke Magome[b], Chikako Moriyoshi[b], Yoshihiro Kuroiwa[b], Takei Takahiro[c], and Nobuhiro Kumada[c]

Affiliations: a) Division of Materials Chemistry, Faculty of Engineering, Hokkaido University, Kita 13 Nishi8, Kita-ku, Sapporo 060-8628, Japan, b) Department of Physical Science, Hiroshima University, 1-3-1 Kagamiyama, Higashihiroshima, Hiroshima 739-8526, Japan, c) Center for Crystal Science and Technology, University of Yamanashi, 7-32 Miyamae, Kofu 400-8511, Japan

Tel: +81-11-706-6578

E-mail: amiura@eng.hokudai.ac.jp

Abstract: Crystallographic and electronic structures of Nb-, Mo-, Ta-, and W-based layered oxides, oxynitrides, and nitrides were analyzed to elucidate the structural relationship between layered oxides and nitrides consisting of octahedral and trigonal-prismatic layers. The electron density, as derived by synchrotron X-ray analysis of $LiNbO_2$ and $Ta_{5-x}(O,N)_6$, showed orbital overlaps between Nb–Nb and Ta–Ta metals in the trigonal layers. Computational calculations based on DFT exhibited that these overlaps stabilized these structures by lowering the hybridization states composed of the d_{xy}, $d_{x^2-y^2}$, and d_{z^2} orbitals below the Fermi level. The crystal structures and formation energies suggest that tuning the Fermi level through the substitutions and vacancies of the cation/anion sites determines the structural preferences of the coordination. The properties and syntheses of these compounds are briefly described. This study enhances the understanding of layered oxides, oxynitrides, and nitrides to further the development of new synthetic approaches, compounds, and applications.

Keywords: X-Ray diffraction, First-principles calculations, Maximum entropy method, Layered structure, Metal-metal bonding

1. Introduction

Layered oxides are attractive materials because of their anisotropic structures and properties. For instance, after the discovery of superconductive quaternary and higher oxides with layered structures, many studies have been performed on complicated layered oxides [1-5]. In these complicated materials, defects and substitution are the key routes to tuning their anisotropic properties, and many studies have focused on controlling the vacancies, coordination, and substitution of the cation and anion sites. Recently, the effects of the anion species, such as F^{-}, O^{2-}, S^{2-}, Se^{2-}, N^{3-}, P^{3-}, and As^{3-}, on the properties of inorganic materials have received significant attention [6-9]. Among them, the nitride anion (N^{3-}) is one of the most similar anions to the oxide anion (O^{2-}) in terms of ion size, polarization, and electronegativity. Thus, in a few decades, many ternary nitrides or oxynitrides with layered structures have been discovered [10-12]. The chemical and physical properties of these layered nitrides/oxynitrides have been examined for their potential applications, such as in lithium ion batteries, superconductors and photovoltaics, catalysts and thermoelectronics.

Some binary, ternary, and more complicated oxides and nitrides with early 4d and 5d transition metals adopt relatively simple layered ABX_2 oxide, oxynitride, and nitride structures (A: Li, Na, Mg, Ca, Sc, Mn, Fe, Cu, Ag, Nb, Mo, Ta, W; B: Nb, Mo, Ta, W, X: O, N). For example, $NaNbO_2$ has a layered structure consisting of octahedral Na–O and trigonal-prismatic Nb–O layers (Fig. 1) [13]. On the other hand, $NaNbN_2$ contains both octahedral Nb–N and Na–N layers; this can be called a layered

rock-salt structure [14]. The structural difference between octahedral and trigonal-prismatic coordination has been theoretically studied in layered sulfides and selenides by Kertesz and Hoffmann: They attributed the differences to variations in the electron count and overlap of the metal-metal orbitals [15]. Although some studies have computationally predicted this metal-metal overlap [16, 17], it has rarely been experimentally visualized. Compounds beyond layered ABX_2 oxides and nitrides have not been systematically studied, which is necessary for further investigation of related materials.

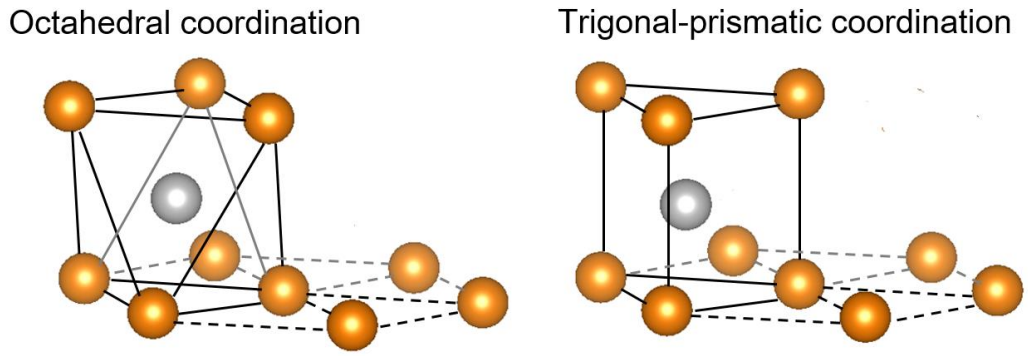

Figure 1 Scheme of octahedral and trigonal coordination.

In this work, the crystal structures and bonding features of layered ABX_2 oxides, oxynitrides, and nitrides are examined. First, we focus on $LiNbO_2$ and Ta_5N_6 as examples of layered structures with octahedral and trigonal-prismatic layers. Analysis of their synchrotron X-ray powder diffraction patterns experimentally reveals the metal-metal bonding within the trigonal prism in real space, and computational calculations show that this orbital overlap stabilizes these layered structures. Next, we determine the relationship between the electron count and coordination by analyzing various related oxides, oxynitrides, and nitrides. In the final section, the properties of the related layered oxides,

oxynitrides, and nitrides are summarized to provide clues for exploring new synthetic approaches, unrevealed compounds, and novel applications.

2. Material and methods

$LiNbO_2$ and $Ta_{5-x}(N,O)_6$ powders were synthesized following preciously reported procedures [18, 19]. Briefly, $LiNbO_2$ was synthesized by heating NbO and Li_3NbO_4 in a vacuumed quartz tube [18]. $Ta_{5-x}(N,O)_6$ was synthesized by thermal ammonolysis of $FeTaO_4$ at 800 °C followed by washing with 1 M HCl aqueous solution to remove the iron byproducts [19]. Chemical analysis was performed by EDX, ICP, and combustion analysis. Synchrotron X-ray analysis was performed at the SPring-8 B02L beam line. Rietveld analysis was performed using RIETAN-FP [20], and the electron density was analyzed using a maximum entropy method (MEM) using Dysnomia [21]. The crystal structures and electron densities were visualized using VESTA [22]. Computational calculations based on density functional theory (DFT) were performed using the VASP package [23] with the GGA-PBE approach [24-26]. *k*-Point meshes of 12 × 12 × 3 and 8 × 8 × 4 were generated for $LiNbO_2$ and Ta_5N_6, respectively [27]. Relaxation of geometry optimization was performed, and a cutoff energy of 400 eV was used. Crystal orbital Hamilton population (COHP) analysis [28] was performed using the TB-LMTO-ASA package [29].

3. Results and Discussion

3.1 Structure and bonding of $LiNbO_2$

We shall start with $LiNbO_2$ consisting of alternate Nb–O trigonal-prismatic and Li–O octahedral layers (Figure 2). Isostructural compounds include many oxides and nitrides, such as Li_xNbO_2 [18], Na_xNbO_2 [30], and $MgMoN_2$ [31]. The Rietveld refinement profile of the X-ray diffraction of the synthesized $LiNbO_2$ powder showed the reported $LiNbO_2$ phase with approximately 1 mass% of NbO_2 [32] as an impurity. The lattice parameters (a = 2.91267(2) Å and c = 10.44871(8) Å) and atomic positions were close to those in previous reports [18, 33, 34]. The Li/Nb molar ratio was 0.97, as determined by ICP analysis; since it is close to unity, we performed the analysis with full occupancies for lithium and niobium. The R_{wp} and S values converged to 1.57% and 1.51, respectively.

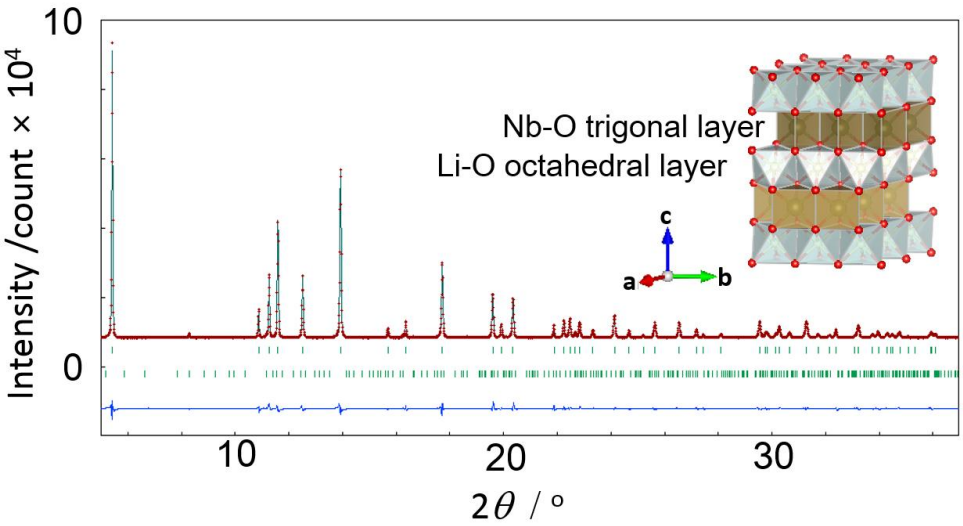

Figure 2 Crystal structure and Rietveld refinement profile of $LiNbO_2$. The structure shows the Nb–O trigonal-prismatic and Li–O octahedral layers. The small spheres represent oxygen atoms. Synchrotron XRD was measured at a wavelength of 0.49607 Å. The upper and lower tic marks represent the position of the allowed reflections for $LiNbO_2$ and NbO_2, respectively.

Experimental visualization of the charge density based on MEM analysis of the diffraction pattern showed good overlap of the orbitals between Nb and O and a localized Li orbital (Fig. 3(a)). As

expected, this electron density indicates a covalent Nb–O bond and a less covalent Li–O bond. The electron density in the Nb plane was clearly higher than that observed in the Li plane (Figs. 3(b) and (c)). Thus, the Nb orbitals overlapped in the trigonal-prismatic plane, while there was minimal overlap of the Li orbitals in the octahedral plane.

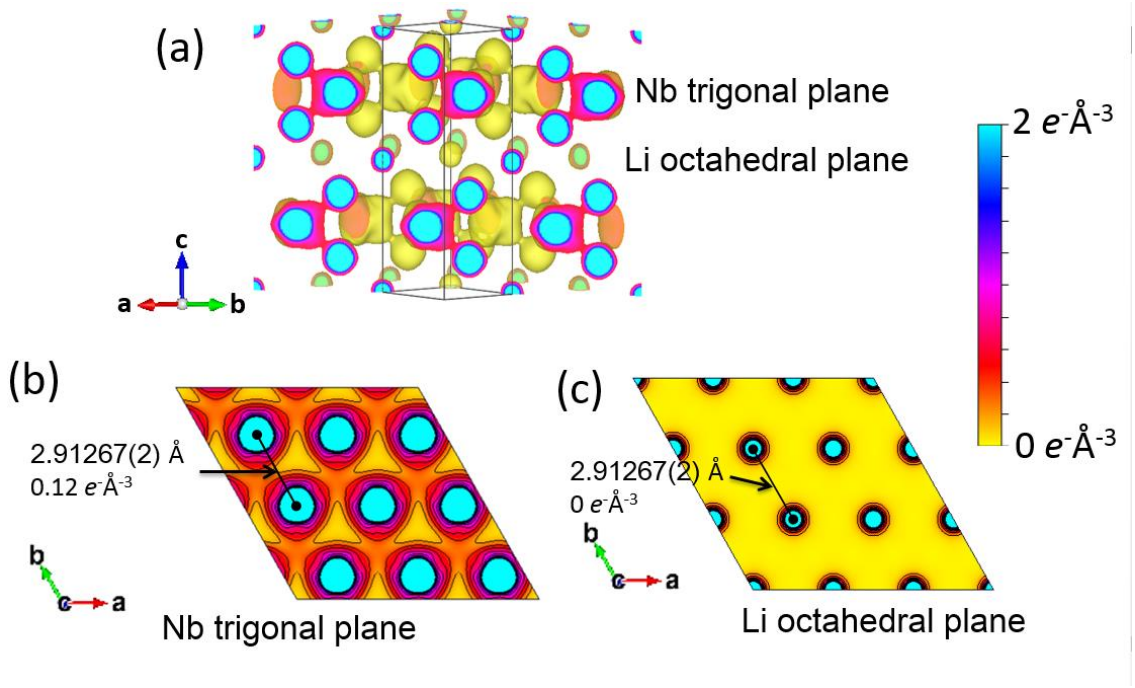

Figure 3 Charge density of $LiNbO_2$ derived by MEM analysis of the synchrotron XRD data. (a) 3D charge density with an isosurface of 0.55 e^{-}Å^{-3}. (b) Nb plane parallel to the c-plane. (c) Li plane parallel to the c-plane.

Computational analysis using DFT supported the experimental MEM analysis (Fig. 4). Near the band gap, the Nb and O states were dominant and overlapped. The projected states of d_{xz} and d_{yz} spread over a wide range by interacting with oxygen orbitals in the trigonal prism. Additionally, the

projected d_{xy}, $d_{x^2-y^2}$, and d_{z^2} states also spread and formed relatively localized states just below the Fermi level. This calculated result is consistent with the previous report regarding Li_xNbO_2 [17] and similar trends can be seen in transition-metal dichalcogenites, such as NbS_2 [15].

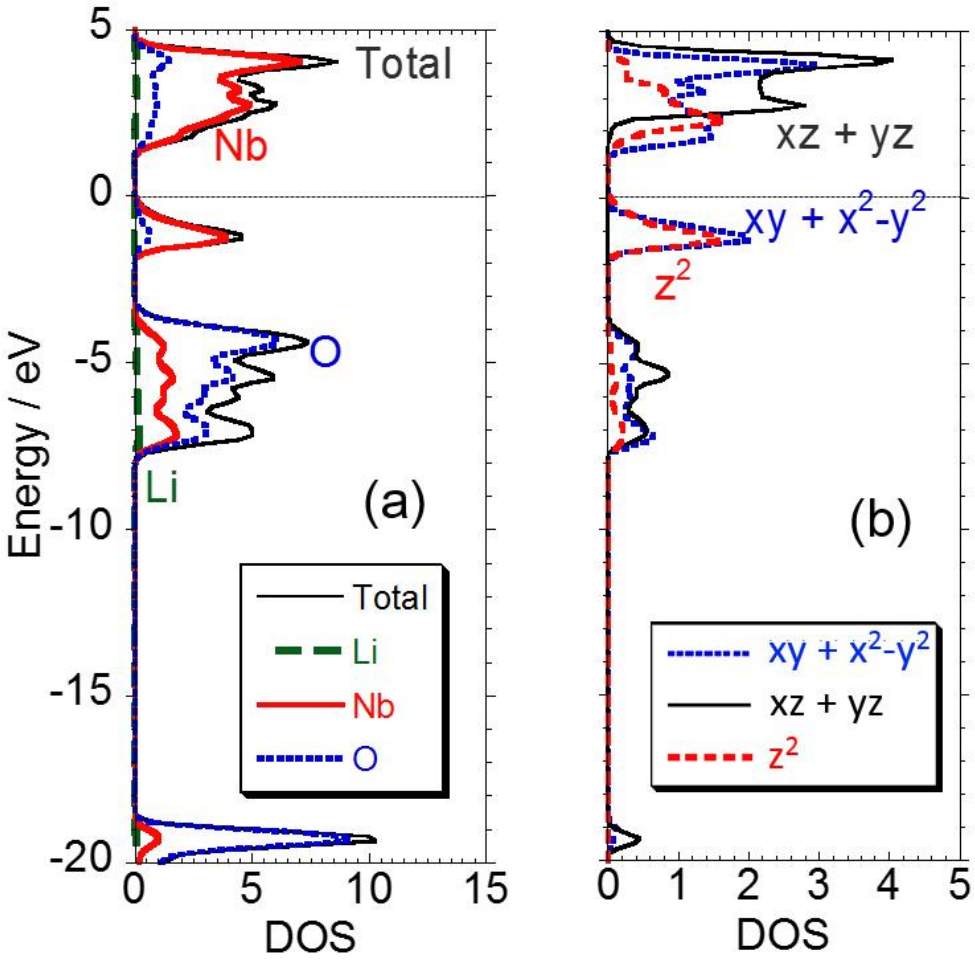

Figure 4 Density of states of $LiNbO_2$ calculated using the VASP code. (a) Total and partial DOS of $LiNbO_2$ and (b) projected DOS into the $d_{xz}+d_{yz}$, $d_{xz}+d_{x^2-y^2}$, and d_{z^2} orbitals. Zero energy is set to the Fermi level.

The overlaps between the Li–O, Nb–O, and Nb–Nb orbitals are shown in the COHP analysis (Fig. 5). A small overlapping population of Li–O bonding states is located around −7 eV, and more overlap between Nb–O and Nb–Nb occurs over a wide range. The state just below the Fermi level consists of

Nb–O anti-bonding interactions and Nb–Nb bonding interactions. Thus, the overlapped orbitals in the Nb plane, which were visualized as high electron density by MEM analysis, would stabilize this layered trigonal-prismatic structure.

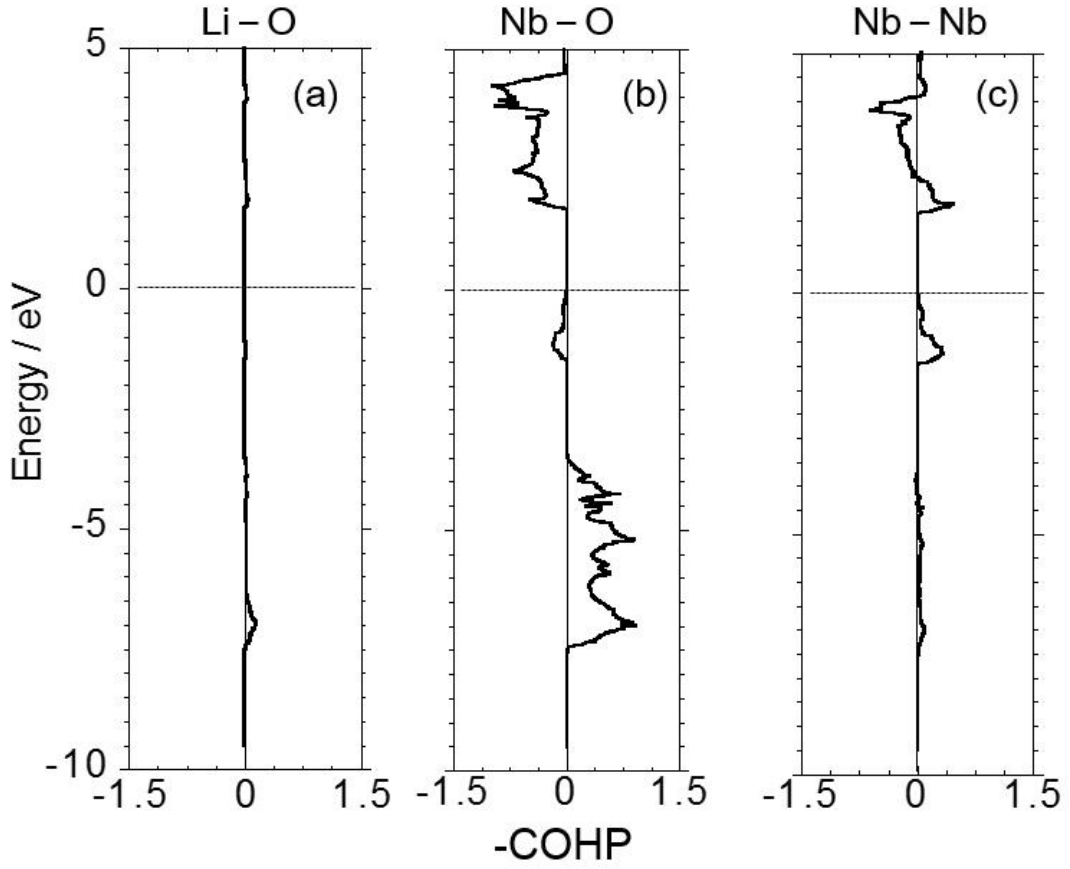

Figure 5 COHP analysis of (a) Li–O, (b) Nb–O, and (c) Nb–Nb bonding within $LiNbO_2$ performed using TB-LMTO-ASA code. Zero energy is set to the Fermi level.

3.2 Structure and bonding of nitrogen-rich $Ta_{5-x}(N,O)_6$

The crystal structure of Ta_5N_6 consists of trigonal-prism and octahedral Ta–N layers with vacancies and slightly off-center Ta positions (Fig. 6) [19]. We can describe Ta_5N_6 as $(Ta_{0.67}\square_{0.33})_{oct}(Ta)_{tri}N_2$, in which the octahedral position comprises one third of the ordered vacancies, while the trigonal position is fully occupied. The trigonal position of Ta is slightly off-center in the trigonal

plane and forms Ta trimers. There are several related compounds, such as $Nb_5(O,N)_{6-x}$ [19], $Ta_5(O,N)_{6-x}$ [19], $LiNb_3N_4$ [35, 36], $(Li_{0.88}\square_{0.12})Nb_{3.0}(O_{0.13}N_{0.87})_4$ [37], and Mo_5N_6 [38].

Figure 6 shows the Rietveld refinement of X-Ray diffraction pattern of $Ta_{5-x}(O,N)_6$ powder synthesized via thermal ammonolysis of $FeTaO_4$ followed by an acid wash. The major peaks were assigned as a hexagonal cell. Nonetheless, minor unindexed peaks were also observed. These may be assigned as the α-TaON phase with a hexagonal structure even though the electronic calculations do not support the existence of this phase [39]. EDX analysis showed that the ratio of Fe/Ta was semi-quantitatively less than 0.01. Combustion analysis showed 8.3 wt% nitrogen and 1.0 wt% oxygen. Assuming that the combustion residual was Ta, the Ta/N/O molar ratio was 1:1.20:0.13; this ratio is close to the theoretical value for Ta_5N_6, which indicates that the major phase should be close to Ta_5N_6. Fe and O may be present as impurity phases, as an amorphous oxidized layer, or incorporated into Ta or N sites in Ta_5N_6. Since partial incorporation of oxygen cannot be disproven, we shall describe the major phase as $Ta_{5-x}(O,N)_6$, i.e., a nitrogen-rich layered tantalum oxynitride with trigonal-prismatic layers.

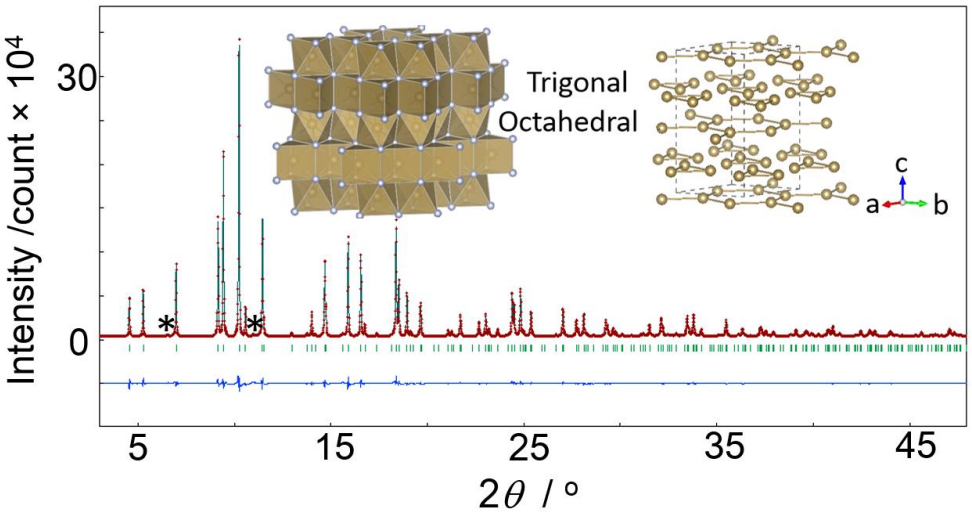

Figure 6 Crystal structure and Rietveld refinement profile of $Ta_{5-x}(O,N)_6$ (x ≈ 0.18). The structure shows a Ta–(O,N) trigonal-prismatic layer and octahedral layer with ordered vacancies. The small spheres represent oxygen/nitrogen atoms. Synchrotron XRD was measured at a wavelength of 0.41365 Å. The tic marks and line below the pattern represent the positions of the allowed reflections for $Ta_{5-x}(O,N)_6$ and difference between the observed and calculated profiles, respectively. The asterisk indicates an impurity phase(s).

Rietveld refinement showed lattice parameters (a = 5.18369 (4) Å and c = 10.36567(8) Å) and atomic positions similar to those reported previously for Ta_5N_6 and $Ta_5(O,N)_6$ [19]. Refinement of the occupation of the trigonal Ta site revealed that it was unity and formed triangle trimers by a slight shift parallel to the c-plane [19]. The distances of the shorter Ta–Ta bonds in the trimers and longer bonds between the trimers were 2.9072(6) and 3.0365(6) Å, respectively. The octahedral sites were found to have ordered and disordered vacancies; the ordered vacancies comprised one third of the octahedral sites (2*a* site) [19], while the disordered vacancies comprised ~9% of the 4*d* site, which had not been reported previously. The Ta–Ta distance in the octahedral layer was 2.9928(3) Å. The equivalent isotropic atomic displacement parameter, B_{eq}, of the octahedral site (0.543(12) Å^2) was

much higher than that of the trigonal site (0.056(6) $Å^2$), which could be related to the vacancies and decreased metal-metal overlap in the octahedra, as described below. The final R_{wp} and S values were 4.88% and 4.35, respectively.

The electron density derived from MEM analysis of the diffraction peaks is shown in Fig. 7. Both the trigonal and octahedral layers showed connected electron density between the Ta and (N,O) atoms. The electron densities in the trigonal and octahedral planes parallel to the *xy* plane were different. The trigonal sites showed a high electron density between Ta sites within the trigonal trimer. The minimum electron densities of Ta–Ta for the shorter bond in the trimers and longer bond between trimers were 0.51 and 0.26 $e^{-}Å^{-3}$, respectively. In contrast, the electron density between the Ta atoms in the octahedral layer was 0.29 $e^{-}Å^{-3}$. Thus, the Ta–Ta interactions in Ta trimers in the trigonal prism would have more covalent characteristics than those in the octahedral layer.

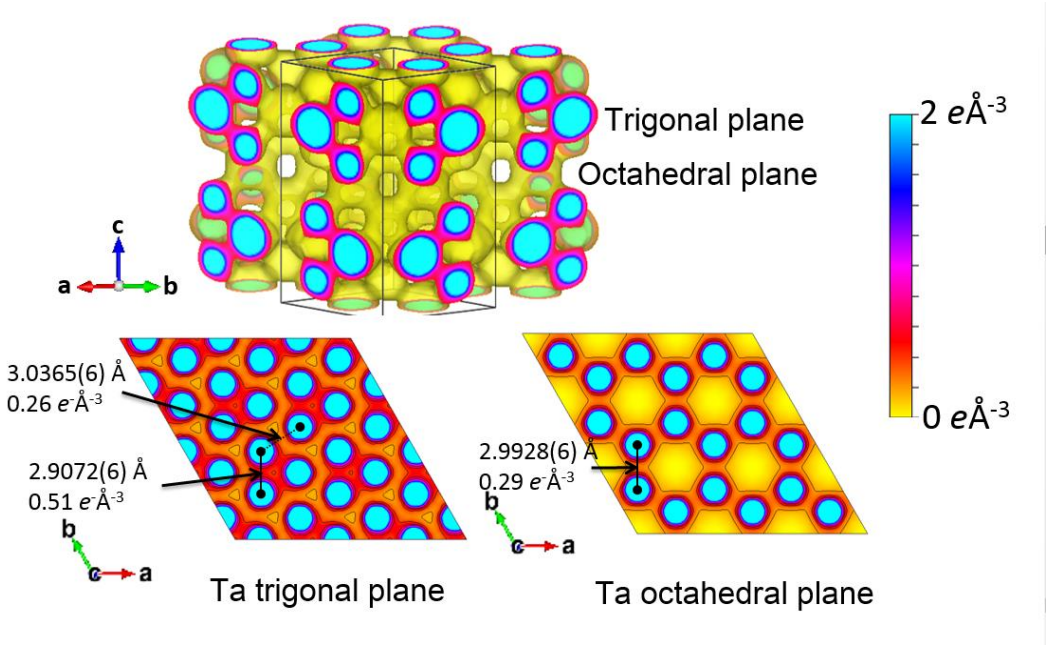

Figure 7 Charge density of $Ta_{5-x}(O,N)_6$ derived by MEM analysis of synchrotron XRD data. (a) 3D charge density with an isosurface of 0.55 $Å^{-3}$. (b) Ta trigonal plane parallel to the c-plane. (c) Ta octahedral plane parallel to the c-plane.

Ta_5N_6 was further analyzed by computational calculations: Its trigonal site was fully occupied, and only ordered octahedral vacancies formed in the octahedral layer. Figure 8 shows the pDOS of Ta_5N_6. The Ta 5d and N 2p orbitals overlapped well and formed states within a wide range. The pDOS of the octahedral and trigonal Ta states showed characteristic features of their trigonal and octahedral coordination spheres; in both, the d_{xz}+d_{yz} orbitals were separated, similar to in $LiNbO_2$. The states that were mainly composed of d_{xy}+$d_{x^2-y^2}$ and d_{z^2} orbitals near the Fermi level were significantly different in the trigonal and octahedral layers: The trigonal layer formed these states around −3 and 4 eV while those in the octahedral layer formed at −0.5–3 eV. The greater separation of the states in the trigonal layer could be explained by the greater overlap between Ta–Ta orbitals, which was experimentally visualized by MEM analysis.

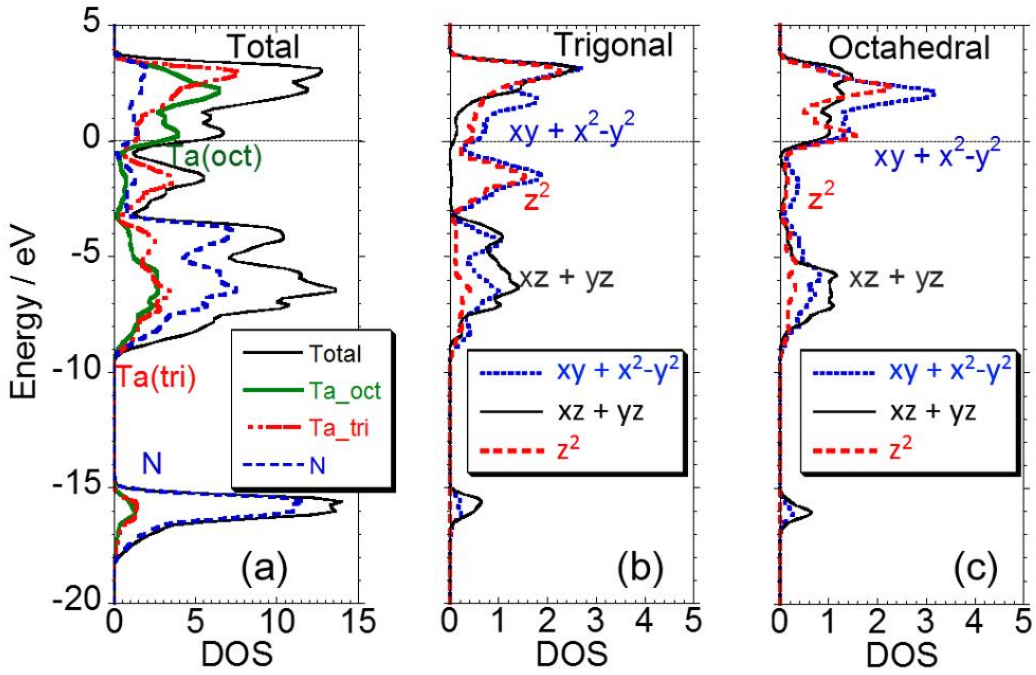

Figure 8 DOS of Ta_5N_6 calculated using the VASP code. (a) Total and partial DOS of Ta_5N_6 projections into the $d_{xz}+d_{yz}$, $d_{xz}+d_{x^2-y^2}$, and d_{z^2} orbitals of Ta in the (b) octahedral and (c) trigonal sites. Zero energy is set to the Fermi level.

Figure 9 shows the COHP analysis of Ta_5N_6, which exhibited similar trends for the Ta–N bonds in the octahedral and trigonal coordination sites, but different features for the Ta–Ta bonds. The Ta–N bonds in both coordination show bonding and anti-bonding interactions below and above the Fermi level, respectively. For the Ta–Ta bonds in the octahedral site, there was only slight electron occupation of the states from bonding interactions. In the trigonal site, two different Ta–Ta bonds formed because of the slightly off-center position of the Ta atom. As expected, shorter bonds resulted in greater overlap of the Ta–Ta orbitals (solid line) and vice versa (dotted line). These bonding populations were located below the Fermi level; thus, the interactions between Ta–Ta orbitals in the trigonal trimer would stabilize this layered structure.

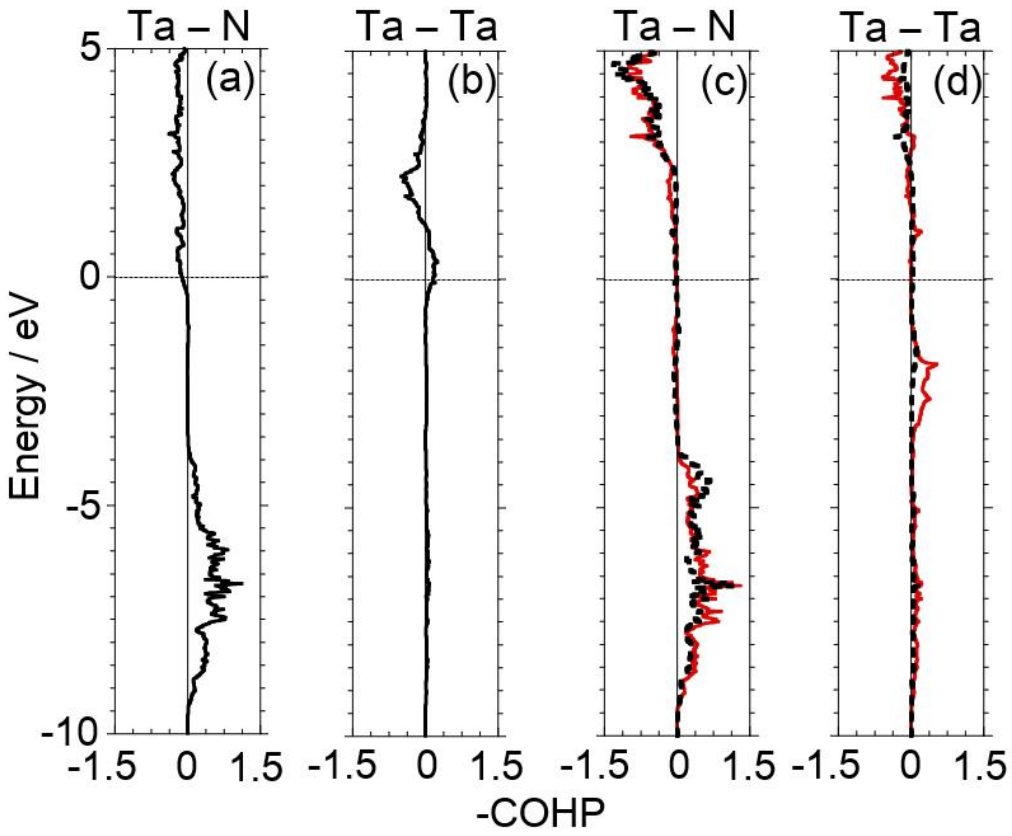

Figure 9 COHP analysis using TB-LMTO-ASA code of (a) Ta–N and (b) Ta–Ta bonds in the octahedral layer and (c) Ta–N and (d) Ta–Ta bonds in the trigonal-prismatic layer within Ta_5N_6. The solid and dotted lines indicate the shorter bonds that form the trimers and longer bonds between trimers due to the slightly off-centered Ta in the trigonal prism, respectively. Zero energy is set to the Fermi level.

To understand the effects of the vacancies, the formation energies of Ta_xN_6 with different vacancies were calculated (Fig. 10): Ta_6N_6 is the structure with no vacancies, while Ta_3N_6 has full vacancies of either the octahedral or trigonal sites. Our results showed that Ta_xN_6 became increasingly unstable with increasing concentration of trigonal vacancies and more stable upon the introduction of one third of the vacancies in the octahedral site, as was exhibited experimentally. This can be explained by the fully filled states formed via bonding interactions between Ta atoms in the trigonal layer, as

described. Thus, a one third vacancy in the octahedral sites is preferable to that in the trigonal sites in this layered structure.

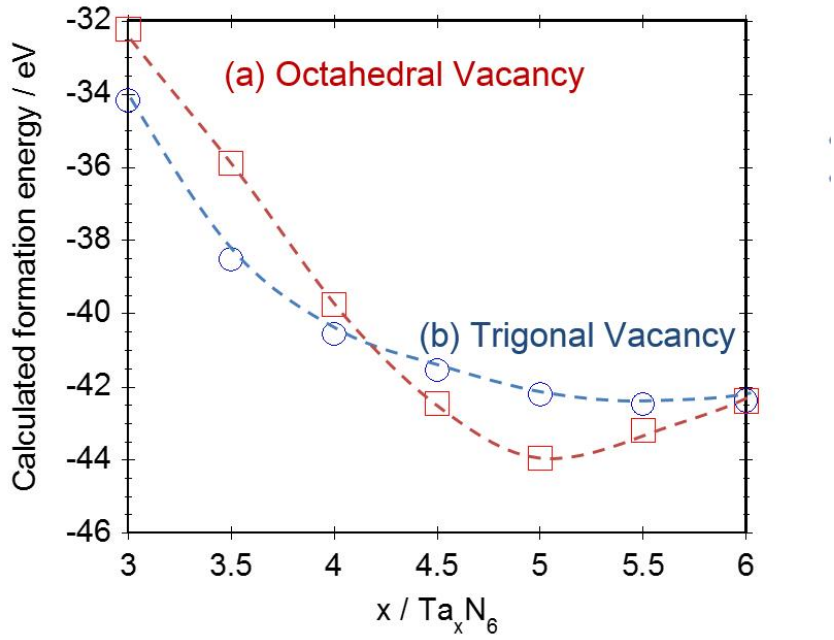

Figure 10 Formation energies of Ta_xN_6 with (a) fully occupied trigonal sites with octahedral vacancies and (b) fully occupied octahedral sites with trigonal vacancies calculated by the VASP code.

3.3 Electron count and structure of ABX_2 compounds

Structural study of $LiNbO_2$ and $Ta_{5-x}(O,N)_6$ revealed that the trigonal prism formed from metal-metal bonds. The metal-metal bonds placed the hybridized states of the d_{xy}, $d_{x^2-y^2}$, and d_{z^2} orbitals below the Fermi level; thus, these layered structures were stabilized. Similar explanation have been reported regarding calcogenides, such as NbS_2 and $NbSe_2$, using a computational approach [15]. It has been found that hybridization of the d_{xy}, $d_{x^2-y^2}$, and d_{z^2} orbitals is enhanced by the formation of trigonal prisms when their electron count is well below the Fermi level [15]. We may expect that similar trends may occur in ABX_2 oxides, oxynitrides, and nitrides with different cations and anions.

Table 1 Reported ABX_2 oxides, oxinitrides, and nitrides with d electron counts and BX_2 coordination assuming a charge transfer from the alkali/alkali-earth metals/Sc^{3+} and O^{2-}/N^{3-} ions to Nb/Mo/Ta/W.

d electron	Formula	BX_2	Refs
0	$NaNbN_2$	Octahedral	[14]
0	$NaTaN_2$	Octahedral	[40]
1	$CaTaN_2$	Octahedral	[41]
1	$LiMoN_2$	Trigonal	[42]
1	$LiWN_2$	Trigonal	[43]
1.33	$Li_{0.5}Nb_{1.5}N_2$ $(Li_{0.5}\ Nb_{0.5})NbN_2$	Trigonal	[35, 36]
1.33	$Li_{0.5}Ta_{1.5}N_2$ $(Li_{0.5}Ta_{0.5})TaN_2$	Trigonal	[44]
1.4	Nb_5N_6 $(Nb_{0.67}\square_{0.33})NbN_2$	Trigonal	[19]
1.4	Ta_5N_6 $(Ta_{0.67}\square_{0.33})TaN_2$	Trigonal	[19]
1.5	$Mg_{1-x}Ta_{2+x}N_3$ $(Mg_{0.67}Ta_{0.33})TaN_2$: x~0	Trigonal	[44]
1.55	$Li_{0.84}W_{1.16}N_2$ $(Li_{0.84}\ W_{0.16})WN_2$	Trigonal	[45]
2	$ScTaN_2$	Trigonal	[16]
2	$MgMoN_2$	Trigonal	[31]
2	$LiNbO_2$	Trigonal	[33]
2	$NaNbO_2$	Trigonal	[13]
2	$Mg_{0.5}NbO_2$ $(Mg_{0.5}\ \square_{0.5})NbO_2$	Trigonal Trigonal	[46]
2	$CaNb_2O_4$ $(Ca_{0.5}\ \square_{0.5})NbO2$	Trigonal	[47]
2.4	Mo_5N_6 $(Mo_{0.67}\square_{0.33})MoN_2$	Trigonal	[38]
3	$LiMoO_2$	Octahedral	[48]
3	$NaMoO_2$	Octahedral	[49]

Table 1 shows a list of ABX_2 oxides, oxynitrides, and nitrides and their BX_2 coordination and d electron count assuming charge transfer from the alkali/alkali-earth metals and O^{2-}/N^{3-} ions to Nb/Mo/Ta/W. The main conclusions are as follows:

1. Compounds with electron counts of around 1–2.4 formed layered structures with trigonal prism coordinations.
2. The trends were not strongly related to the cation and anion species and vacancies.

To confirm these experimental trends, we calculated the differences in the formation energies of various ABX_2 compounds with various cations (A site: alkali/alkali-earth metals; B site: Nb, Mo) and anions (X site: N/O), which were isostructural with $NaNbN_2$ (octahedral) and $NaNbO_2$ (trigonal). Figure 11 reveals that the trigonal-prism coordination is stabilized in the range of electron counts between 1 and 2.7; this is similar to what has been reported experimentally (Table 1). This trend is also similar to the computational calculations of transition-metal calcogenides, which was explained by stabilization of the trigonal structure by the formation of metal-metal bonds with suitable Fermi levels [15].

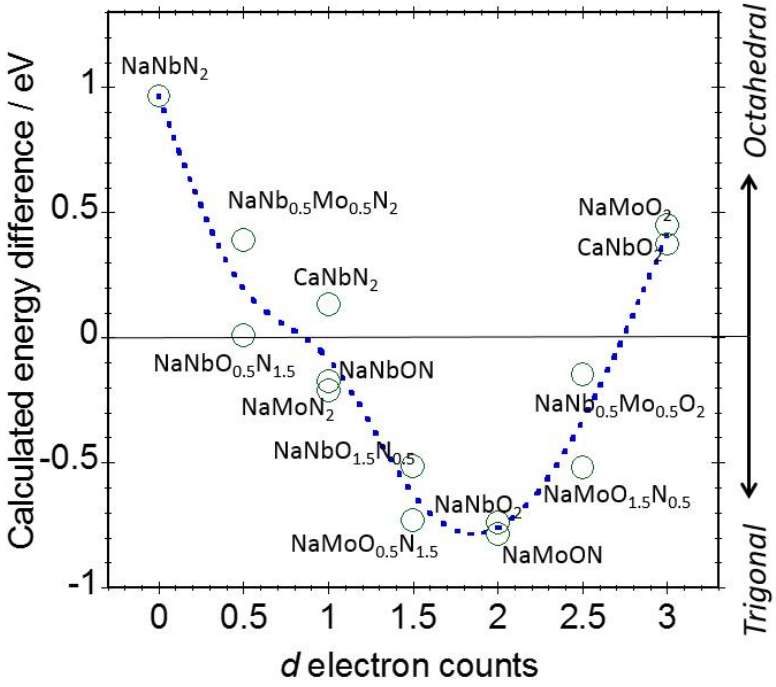

Figure 11 Formation energy differences of various ABX_2 oxides, oxynitrides, and nitrides that are isostructural with $NaNbN_2$ (octahedral) and $NaNbO_2$ (trigonal) calculated using the VASP code. A charge transfer from the alkali/alkali-earth metals and O^{2-}/N^{3-} ions to Nb/Mo is assumed to calculate d electron counts. Some of these compounds are hypothetical and have not been experimentally reported. The dashed line is provided to guide the eye.

It is possible to assess this relationship between electron counts and structures in compounds with 3d transition metals in the A sites, such as $FeWN_2$ [50-53], $MnWN_2$ [54], and $MnMoN_2$ [50]. These materials have layered structures consisting of octahedral layers with 3d transition metals and trigonal-prismatic layers with 4d or 5d metals. The 3d metals can be considered to be divalent cations considering their ionic radii, and, if so, the electron count of the d orbitals of Mo and W would be close to d^2 and these could follow the structural rule found in this work, i.e., the relationship between the d electron count of the 4d/5d metal and octahedral/trigonal coordination. Their octahedral sites might be somewhat flexible with respect to the vacancies, and substitution in the octahedral sites has

been reported in Fe_xWN_2 [55, 56], $(Fe_{0.8}Mo_{0.2})MoN_2$ [57], $(Fe_{0.8}W_{0.2})WN_2$ [58], and $(Co_{0.6}Mo_{0.4})MoN_2$ [59, 60].

Additionally, some nitrides with monovalent transition metals (i.e., Cu/Ag) can be understood similarly, e.g., $CuNbN_2$ [61, 62], $CuTaN_2$ [63], and $AgTaN_2$ [64, 65]. We could treat these as d^0 compounds, and they have octahedral (Nb/Ta)–N planes, as expected. Nonetheless, these compounds have linear Ag/Cu–N bonds, which are commonly seen in delafossite oxides, such as $AgCoO_2$ [66].

3.4 Remarks on the properties and syntheses of ABX_2 compounds

In the previous section, the coordination and vacancies of these layered ABX_2 oxides, nitrides, and oxynitrides were found to be related to both the anion and cation species; this relationship suggests that the properties of these compounds are affected by these species, and thus their syntheses should be performed with control of the anion and cation species. Herein, we describe a short description of the properties and syntheses of ABX_2 oxides, oxynitrides, and nitrides to help further exploration of related materials.

The d^0 nitrides show semiconductive behavior, and their visible or infrared absorption properties show the potential for solar energy conversion [61, 62]. $SrZrN_2$ and $SrHfN_2$, which are isostructural with $NaNbN_2$, have been computationally predicted to be thermoelectronic materials [67]. The d^1 and d^2 nitrides, oxynitrides, and oxides show metallic or semiconductive transport properties depending on their electron counts and hybridization of the orbitals. Some of these compounds show

superconductive properties, including Li_xNbO_2 ($T_c \approx 5$ K) [68], Na_xNbO_2 ($T_c \approx 4$ K) [30], $CaTaN_2$ ($T_c \approx 9$ K) [41], and $(Li_{0.88}\square_{0.12})Nb_{3.0}(O_{0.13}N_{0.87})_4$ ($T_c \approx 3$ K) [37]. The electrochemical performances of Li_xMoN_2 [42], Li_xWN_2 [69], and Li_xMoO_2 [70] have been examined for potential applications as electrodes for rechargeable lithium batteries. Ferromagnetic-like properties have been found in $Fe_{0.74}WN_2$ with defective Fe triangles [56]. The electrocatalytic properties of $Co_{0.6}Mo_{1.4}N_2$ for hydrogen evolution reaction and oxygen reduction reaction have been examined [59, 60]. Even though there are potential applications, most of the reported properties include the effects of the surface layers, impurities, and grain connections. For the synthesis of oxynitrides and nitrides, a major approach is to heat (typically above 600–1000 °C) the oxide, sulfide, or chloride precursors under an ammonia flow; in these reactions, the temperature profile and ammonia flow rate should be kinetically controlled [12, 71-73]. Single crystals of several ABX_2 compounds have been grown using flux methods ($LiNbO_2$ [74, 75], $CaNb_2O_4$ [47], and $NaNbN_2$ [76]); however, many ABX_2 compounds are only available in the powder form. Therefore, further development of synthetic techniques to control the cationic and anionic species and morphologies are important for finding new compounds and examining the intrinsic properties and exploring new applications of these ABX_2 compounds.

4. Conclusions

The structural preferences and bonding of various ABX_2 oxides and nitrides consisting of octahedral and trigonal-prismatic layers were investigated. In both the oxides and nitrides, the

octahedral and trigonal coordinations were closely related to the Fermi level, which was controlled by the anions, cations, and vacancies. The trigonal layer formed metal-metal bonds, which lowered the hybridized states composed of $d_{xz} + d_{x^2-y^2}$ and d_{z^2} orbitals below the Fermi level. Layered structures with prismatic-trigonal coordination formed when the d electron count was around 1–2.5 assuming charge transfer from the alkali or alkali-earth metals. The structures of the ABX_2 compounds together with their synthetic routes and magnetic and electronic properties were summarized. This work elucidated a systematic trend for understanding layered oxides, oxynitrides, and nitrides consisting of octahedral and trigonal-prismatic layers, which is important for further exploration of new layered compounds and their properties by mixing cations and anions and controlling vacancies.

Acknowledgements

A. M. acknowledges Prof. S. Kikkawa for fruitful discussions. The experiments at SPring-8 were performed with the approval of the JASRI (proposal numbers 2014A1008 and 2014B1071).

Supplementary material

Detailed results of the Rietveld refinement of $LiNbO_2$ and $Ta_{5-x}(O,N)_6$ are summarized in the supporting material.

References

[1] J.G. Bednorz, K.A. Müller, Possible highT c superconductivity in the Ba−La−Cu−O system, Zeitschrift für Physik B Condensed Matter, 64 (1986) 189-193.

[2] C.W. Chu, L. Gao, F. Chen, Z.J. Huang, R.L. Meng, Y.Y. Xue, Superconductivity above 150 K in HgBa2Ca2Cu3O8+[delta] at high pressures, Nature, 365 (1993) 323-325.

[3] M. Wu, J. Ashburn, C. Torng, P. Hor, R. Meng, L. Gao, Z. Huang, Y. Wang, C. Chu, Superconductivity at 93 K in a new mixed-phase Y-Ba-Cu-O compound system at ambient pressure, Phys. Rev. Lett., 58 (1987) 908-910.

[4] H. Maeda, Y. Tanaka, M. Fukutomi, T. Asano, A New High-$T_{¥text{c}}$ Oxide Superconductor without a Rare Earth Element, Japanese Journal of Applied Physics, 27 L209.

[5] N. Takeshita, A. Yamamoto, A. Iyo, H. Eisaki, Zero Resistivity above 150 K in HgBa2Ca2Cu3O8+δat High Pressure, J. Phys. Soc. Jpn., 82 (2013) 023711.

[6] Y. Kamihara, T. Watanabe, M. Hirano, H. Hosono, Iron-Based Layered Superconductor La[O1-xFx]FeAs (x = 0.05-0.12) with Tc = 26 K, J. Am. Chem. Soc., 130 (2008) 3296-3297.

[7] Y. Mizuguchi, H. Fujihisa, Y. Gotoh, K. Suzuki, H. Usui, K. Kuroki, S. Demura, Y. Takano, H. Izawa, O. Miura, BiS2-based layered superconductor Bi4O4S3, Physical Review B, 86 (2012).

[8] S.J. Clarke, P. Adamson, S.J.C. Herkelrath, O.J. Rutt, D.R. Parker, M.J. Pitcher, C.F. Smura, Structures, Physical Properties, and Chemistry of Layered Oxychalcogenides and Oxypnictides, Inorg. Chem., 47 (2008) 8473-8486.

[9] Y. Tsujimoto, K. Yamaura, E. Takayama-Muromachi, Oxyfluoride Chemistry of Layered Perovskite Compounds, Applied Sciences, 2 (2012) 206-219.

[10] N. Tapia-Ruiz, M. Segalés, D.H. Gregory, The chemistry of ternary and higher lithium nitrides, Coord. Chem. Rev., 257 (2013) 1978-2014.

[11] S. Ida, Y. Okamoto, M. Matsuka, H. Hagiwara, T. Ishihara, Preparation of tantalum-based oxynitride nanosheets by exfoliation of a layered oxynitride, CsCa2Ta3O(10-x)N(y), and their photocatalytic activity, J Am Chem Soc, 134 (2012) 15773-15782.

[12] A. Fuertes, Chemistry and applications of oxynitride perovskites, J. Mater. Chem., 22 (2012) 3293.

[13] G. Meyer, R. Hoppe, Über Oxoniobate (III). II [1, 2]. Notiz zur Kenntnis von NaNbO2, Z. Anorg. Allg. Chem., 424 (1976) 128-132.

[14] P.E. Rauch, F.J. DiSalvo, Ambient pressure synthesis of ternary group(V) nitrides, J. Solid State Chem., 100 (1992) 160-165.

[15] M. Kertesz, R. Hoffmann, Octahedral vs. trigonal-prismatic coordination and clustering in transition-metal dichalcogenides, J. Am. Chem. Soc., 106 (1984) 3453-3460.

[16] R. Niewa, D.A. Zherebtsov, W. Schnelle, F.R. Wagner, Metal–Metal Bonding in ScTaN2. A New Compound in the System ScN–TaN, Inorg. Chem., 43 (2004) 6188-6194.
[17] E.R. Ylvisaker, W.E. Pickett, First-principles study of the electronic and vibrational properties of LiNbO_{2}, Physical Review B, 74 (2006) 075104.
[18] N. Kumada, S. Muramatu, F. Muto, N. Kinomura, S. Kikkawa, M. Koizumi, Topochemical reactions of LixNbO2, J. Solid State Chem., 73 (1988) 33-39.
[19] J.D. Houmes, H.-C.z. Loye, Iron-Promoted Synthesis of Tantalum and Niobium Oxynitrides, J. Solid State Chem., 127 (1996) 267-275.
[20] F. Izumi, K. Momma, Three-dimensional visualization in powder diffraction, Solid State Phenom., 130 (2007) 150-120.
[21] F. Izumi, K. Momma, Three-dimensional visualization of electron- and nuclear-density distributions in inorganic materials by MEM-based technology, IOP Conference Series: Materials Science and Engineering, 18 (2011) 022001.
[22] K. Momma, F. Izumi, VESTA: a three-dimensional visualization system for electronic and structural analysis, J. Appl. Crystallogr., 41 (2008) 653-658.
[23] G. Kresse, J. Hafner, Ab initio molecular dynamics for liquid metals, Physical Review B, 47 (1993) 558-561.
[24] P.E. Blöchl, Projector augmented-wave method, Physical Review B, 50 (1994) 17953-17979.
[25] G. Kresse, D. Joubert, From ultrasoft pseudopotentials to the projector augmented-wave method, Physical Review B, 59 (1999) 1758-1775.
[26] J.P. Perdew, J.A. Chevary, S.H. Vosko, K.A. Jackson, M.R. Pederson, D.J. Singh, C. Fiolhais, Atoms, molecules, solids, and surfaces: Applications of the generalized gradient approximation for exchange and correlation, Physical Review B, 46 (1992) 6671-6687.
[27] H.J. Monkhorst, J.D. Pack, Special points for Brillouin-zone integrations, Physical Review B, 13 (1976) 5188-5192.
[28] R. Dronskowski, P.E. Bloechl, Crystal orbital Hamilton populations (COHP): energy-resolved visualization of chemical bonding in solids based on density-functional calculations, The Journal of Physical Chemistry, 97 (1993) 8617-8624.
[29] R. Tank, O. Jepsen, A. Burkhardt, O.K. Andersen, LMTO, 2000.
[30] M.A. Rzeznik, M.J. Geselbracht, M.S. Thompson, A.M. Stacy, Superconductivity and Phase Separation in NaxNbO2 (x < 1), Angewandte Chemie International Edition in English, 32 (1993) 254-255.
[31] L. Wang, K. Tang, Y. Zhu, Q. Li, B. Zhu, L. Wang, L. Si, Y. Qian, Solid state synthesis of a new ternary nitride MgMoN2 nanosheets and micromeshes, J. Mater. Chem., 22 (2012) 14559-14564.

[32] A.K. Cheetham, C.N.R. Rao, A neutron diffraction study of niobium dioxide, Acta Crystallographica Section B, 32 (1976) 1579-1580.
[33] G. Meyer, R. Hoppe, The First Oxoniobate(; III) LiNbO2, Angewandte Chemie International Edition in English, 13 (1974) 744-745.
[34] H.-F. Roth, G. Meyer, Z. Hu, G. Kaindl, Synthesis, structure, and X-ray absorption spectra of LixNbO2 and NaxNbO2 ($x \leq 1$), Z. Anorg. Allg. Chem., 619 (1993) 1369-1373.
[35] F. Tessier, R. Marchand, Y. Laurent, Preparation of transition metal nitrides using unusual routes, J. Eur. Ceram. Soc., 17 (1997) 1825-1829.
[36] F. Tessier, R. Assabaa, R. Marchand, Mixed valent niobium nitrides and oxynitrides resulting from ammonolysis of alkaline niobates, J. Alloys Compd., 262–263 (1997) 512-515.
[37] T. Motohashi, M. Ito, Y. Masubuchi, M. Wakeshima, S. Kikkawa, Crystal Structure and Superconducting Properties of Hexagonal Lithium–Niobium Oxynitride, Inorg. Chem., 51 (2012) 11184-11189.
[38] R. Marchand, F. Tessier, F. J. DiSalvo, New routes to transition metal nitrides: and characterization of new phases, J. Mater. Chem., 9 (1999) 297-304.
[39] M.-W. Lumey, R. Dronskowski, The Electronic Structure of Tantalum Oxynitride and the Falsification of α-TaON, Z. Anorg. Allg. Chem., 629 (2003) 2173-2179.
[40] H. Jacobs, E. von Pinkowski, Synthese ternärer nitride von alkalimetallen: Verbindungen mit tantal, MTaN2 MIT M [reverse not equivalent] Na, K, RbundCs, Journal of the Less Common Metals, 146 (1989) 147-160.
[41] V. Balbarin, R.B. Van Dover, F.J. Disalvo, The high temperature preparation and property measurements of CaTaN2: A ternary superconducting nitride, J. Phys. Chem. Solids, 57 (1996) 1919-1927.
[42] S.H. Elder, L.H. Doerrer, F.J. Disalvo, J.B. Parise, D. Guyomard, J.M. Tarascon, LiMoN2 - the 1st metallic layered nitride, Chem. Mater., 4 (1992) 928-937.
[43] P.S. Herle, M.S. Hegde, N.Y. Vasanthacharya, J. Gopalakrishnan, G.N. Subbanna, Synthesis, structure, and properties of LiWN2, J. Solid State Chem., 112 (1994) 208-210.
[44] T. Brokamp, H. Jacobs, Darstellung und Struktur einiger Gemischtvalenter ternärer Tantalnitride mit Lithium und Magnesium, J. Alloys Compd., 183 (1992) 325-344.
[45] S. Kaskel, D. Hohlwein, J. Strähle, Study of Ammonolysis Reactions within SituX-Ray Diffraction: Detection and Crystal Structure of Li0.84W1.16N2, J. Solid State Chem., 138 (1998) 154-159.
[46] A. Miura, T. Takei, N. Kumada, Synthesis and crystal structure of Mg0.5NbO2: An ion-exchange reaction with Mg2+ between trigonal [NbO2]− layers, J. Solid State Chem., 197 (2013) 471-474.
[47] N. Kumada, N. Kinomiura, Preparation and Crystal Structure of a New Reduced

Calcium Niobium Oxide: CaNb2O4, J. Solid State Chem., 147 (1999) 671-675.
[48] L.E. Aleandri, R.E. McCarley, Hexagonal lithium molybdate, LiMoO2: a close-packed layered structure with infinite molybdenum-molybdenum-bonded sheets, Inorg. Chem., 27 (1988) 1041-1044.
[49] B.D. Anderson, J.B. Tracy, Nanoparticle conversion chemistry: Kirkendall effect, galvanic exchange, and anion exchange, Nanoscale, 6 (2014) 12195-12216.
[50] D.S. Bem, C.M. LampeOnnerud, H.P. Olsen, H.C. zurLoye, Synthesis and structure of two new ternary nitrides: FeWN2 and MnMoN2, Inorg. Chem., 35 (1996) 581-585.
[51] P. Subramanya Herle, N.Y. Vasanthacharya, M.S. Hegde, J. Gopalakrishnan, Synthesis of new transition metal nitrides, MWN2 (M=Mn, Co, Ni), J. Alloys Compd., 217 (1995) 22-24.
[52] D.S. Bem, H.C.Z. Loye, Synthesis of the new ternary transition-metal nitride FeWN2 via ammonolysisi of a solid-state oxide precursor, J. Solid State Chem., 104 (1993) 467-469.
[53] D.S. Bem, J.D. Houmes, H.C. zur Loye, In MRS Symposium Proceeding; Covalent Ceramics II: Non-Oxides; Barron, A. R., Fischman, G. S., Fury, M. A., Hepp, A. F., Eds.; Boston, 1993, pp. 153-162.
[54] J. Grins, P.-O. Kall, G. Svensson, Synthesis and structural characterisation of MnWN2 prepared by ammonolysis of MnWO4, J. Mater. Chem., 5 (1995) 571-575.
[55] A. Miura, X.-D. Wen, H. Abe, G. Yau, F.J. DiSalvo, Non-stoichiometric FexWN2: Leaching of Fe from layer-structured FeWN2, J. Solid State Chem., 183 (2010) 327-331.
[56] A. Miura, T. Takei, N. Kumada, E. Magome, C. Moriyoshi, Y. Kuroiwa, Crystal structures and ferromagnetism of FexWN2 (x~0.74, 0.90) with defective iron triangular lattice, J. Alloys Compd., 593 (2014) 154-157.
[57] D.S. Bem, H.P. Olsen, H.C. Zurloye, Synthesis and Electronic and Magnetic Characterization of the Ternary Nitride (Fe0.8Mo0.2)MoN2, Chem. Mater., 7 (1995) 1824-1828.
[58] J.D. Houmes, S. Deo, H.C. zurLoye, Synthesis and characterization of the new ternary nitride (Fe0.8W0.2)WN2, J. Solid State Chem., 131 (1997) 374-378.
[59] B. Cao, G.M. Veith, J.C. Neuefeind, R.R. Adzic, P.G. Khalifah, Mixed close-packed cobalt molybdenum nitrides as non-noble metal electrocatalysts for the hydrogen evolution reaction, J Am Chem Soc, 135 (2013) 19186-19192.
[60] B. Cao, J.C. Neuefeind, R.R. Adzic, P.G. Khalifah, Molybdenum nitrides as oxygen reduction reaction catalysts: structural and electrochemical studies, Inorg Chem, 54 (2015) 2128-2136.
[61] M. Yang, A. Zakutayev, J. Vidal, X. Zhang, D.S. Ginley, F.J. DiSalvo, Strong optical absorption in CuTaN2 nitride delafossite, Energy & Environmental Science, 6 (2013) 2994-2999.

[62] A. Zakutayev, C.M. Caskey, A.N. Fioretti, D.S. Ginley, J. Vidal, V. Stevanovic, E. Tea, S. Lany, Defect Tolerant Semiconductors for Solar Energy Conversion, The Journal of Physical Chemistry Letters, 5 (2014) 1117-1125.
[63] U. Zachwieja, H. Jacobs, CuTaN2, a Copper(I)-Tantalum (V)-Nitride with Delafossite Structure, Eur. J. Solid State Inorg. Chem., 28 (1991) 1055-1062.
[64] A. Miura, M. Wessel, R. Dronskowski, Calculation of the electronic structure of delafossite AgTaN2 from first principles, J. Ceram. Soc. Jpn., 119 (2011) 663-666.
[65] A. Miura, M. Lowe, B.M. Leonard, C.V. Subban, Y. Masubuchi, S. Kikkawa, R. Dronskowski, R.G. Hennig, H.D. Abruña, F.J. DiSalvo, Silver delafossite nitride, AgTaN2?, J. Solid State Chem., 184 (2011) 7-11.
[66] R.D. Shannon, C.T. Prewitt, D.B. Rogers, Chemistry of noble metal oxides. II. Crystal structures of platinum cobalt dioxide, palladium cobalt dioxide, coppper iron dioxide, and silver iron dioxide, Inorg. Chem., 10 (1971) 719-723.
[67] I. Ohkubo, T. Mori, Three-dimensionality of electronic structures and thermoelectric transport in SrZrN2 and SrHfN2 layered complex metal nitrides, Inorg Chem, 53 (2014) 8979-8984.
[68] M.J. Geselbracht, T.J. Richardson, A.M. Stacy, Superconductivity in the layered compound LixNbO2, Nature, 345 (1990) 324-326.
[69] A. Kuhn, M. Martín-Gil, S. Kaskel, J. Strähle, F. García-Alvarado, The effect of cationic disordering on the electrochemical performances of the layered nitrides LiWN2 and Li0.84W1.16N2, J. Eur. Ceram. Soc., 27 (2007) 4199-4203.
[70] D. Mikhailova, N.N. Bramnik, K.G. Bramnik, P. Reichel, S. Oswald, A. Senyshyn, D.M. Trots, H. Ehrenberg, Layered LixMoO2 Phases with Different Composition for Electrochemical Application: Structural Considerations, Chem. Mater., 23 (2011) 3429-3441.
[71] R. Marchand, Y. Laurent, J. Guyader, P. L'Haridon, P. Verdier, Nitrides and oxynitrides: Preparation, crystal chemistry and properties, J. Eur. Ceram. Soc., 8 (1991) 197-213.
[72] F. Tessier, R. Marchand, Ternary and higher order rare-earth nitride materials: synthesis and characterization of ionic-covalent oxynitride powders, J. Solid State Chem., 171 (2003) 143-151.
[73] Y. Masubuchi, S.K. Sun, S. Kikkawa, Processing of dielectric oxynitride perovskites for powders, ceramics, compacts and thin films, Dalton Trans, DOI 10.1039/c4dt03811h(2015).
[74] J.D. Greenlee, J.C. Shank, M.B. Tellekamp, B.P. Gunning, C.A.M. Fabien, W.A. Doolittle, Liquid Phase Electro-Epitaxy of Memristive LiNbO2 Crystals, Crystal Growth & Design, 14 (2014) 2218-2222.
[75] P. Bordet, E. Moshopoulou, S. Liesert, J.J. Capponi, Structure and physical properties of Li1−xNbO2 single crystals, Physica C: Superconductivity, 235–240, Part 2 (1994) 745-746.

[76] H. Jacobs, B. Hellmann, Synthesis and structure of a sodium niobium(V) nitride, NaNbN2, J. Alloys Compd., 191 (1993) 51-52.